Asian Journal of Physics Vol. 18, No. 1 (2009) 7-16

Plasmonic superlenses: theory, practice and recent developments

Ciaran P Moore and Richard J Blaikie
MacDiarmid Institute for Advanced Materials and Nanotechnology
Department of Electrical and Computer Engineering, University of Canterbury
Christchurch, New Zealand

The phenomenon of plasmonic resonance has been identified in recent times as a means of breaking the diffraction limit that hinders high performance lithography systems in use today. Experimental results based on interleaved silver and dielectric layers have shown that resolution as low as $\lambda/6$ can be achieved and that 'superlenses' are indeed realisable. However, examples of 'perfect' lenses, predicted to have true, diffraction-free performance, have yet to be fabricated. This paper uses numerical models of silver-dielectric superlenses to explore performance around and beyond the diffraction limit, examining different superlens designs and the reasons behind their specific performance enhancements and limitations.

1 Introduction

In 1968 Veselago [1] examined left-handed materials (LHMs), that is, materials with negative relative permittivity (ε_r) and permeability (μ_r), and found that they could be used to reconstruct the propagating spectrum of an object. He considered a theoretical lens (to which his name was given) made up of a planar slab of LHM with $\varepsilon_r = \mu_r = -1$ and thickness = 2, sandwiched between two slabs of conventional, right-handed materials (RHMs) with $\varepsilon_r = \mu_r = 1$ and thickness = 1 (Fig. 1). Propagating waves experienced a negative phase shift as they travelled through the LHM, the magnitude of which was exactly equal to the cumulative positive phase shift they experienced travelling through the RHM layers. The net result was a cancellation of any phase distortion experienced by the waves as they travelled from one side of the lens to the other (Fig. 1a). Unfortunately, Veselago was unable to test his theory, as he could not find an appropriate LHM, especially one with $\mu_r \leq 0$: they simply do not exist in nature.

It was the start of a new millennium before Pendry [2] resurrected Veselago's theories, proposing that LHMs could be used to achieve a truly perfect lens. He surmised that a Veselago lens could reconstruct the evanescent as well as the propagating spectra of an object (Fig. 1b), predicting that evanescent waves (which carry sub-wavelength data) would grow exponentially within LHMs, given that they decayed exponentially within RHMs (Fig. 2). Furthermore, he realised that negative μ_r was not essential to the operation of such a lens. Provided the operation of the lens was confined near the electrostatic limit, that is, where all lens dimensions are much less than the wavelength of operation, the behaviour of the electrical and magnetic waves within the lens could be decoupled and isolated. Thus the performance of a perfect electromagnetic lens could be approximated by a perfect electric lens (Fig. 3), provided the incident radiation was oriented in such a way that the magnetic waves were parallel to the lens interface (TM polarisation) and therefore were not capable of penetrating the lens.

Pendry's third, and most significant, achievement was the identification of silver as a suitable LHM for a practical electrostatic superlens. Silver has $\mu_r \approx 1$ and negative ε_r at a wavelength of 365 nm (i-line), caused by resonant plasmons that exist on the surface of the silver. The i-line wavelength is significant as

Corresponding author
e – mail : *c.moore@elec.canterbury.ac.nz* (Prof Ciaran P Moore)

it makes silver suitable for lithography applications with operating wavelengths in or near the visible spectrum. Composite metamaterials, made up of nanoscale rods [3, 4], split ring resonators [5] or combinations of the two [6-8], had been proposed as LHMs before, but their operating wavelengths were all well above the visible range. The identification of silver meant that superlens experiments could be attempted in the optical spectrum and the diffraction limit could be challenged at wavelengths that were relevant to modern lithographic techniques.

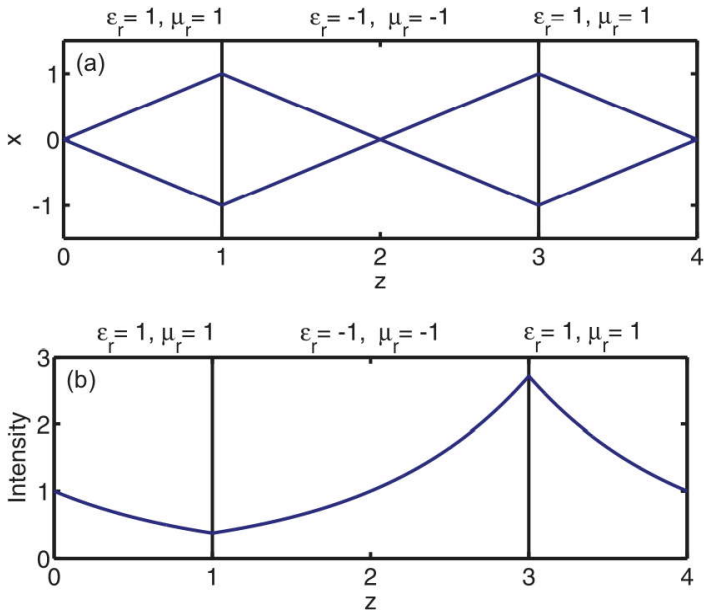

Fig. 1: Veselago lens made up of a slab of theoretical LHM sandwiched between two RHM slabs. The slab's thickness ratio is 1:2:1. Ray diagrams for propagating waves travelling from the object (z = 0) to the image (z = 4) are shown in (a). The changes in intensity that evanescent waves experience on the same journey are shown in (b).

Experimental verification of Pendry's silver-based superlens was followed in 2005. Two groups described super-resolution of 145 nm [9] and 120 nm [10] period structures at an operating wavelength of 365 nm, corresponding to resolution of $\lambda/5$ and $\lambda/6$ features, respectively. However, unlike the perfect lens about which Pendry had theorised, these lenses had resolution improvements of less than an order of magnitude over conventional lenses. This paper reviews the reasons behind this limited increase in performance and examines alternate superlens designs that were proposed to lift real-world performance to the heights predicted by theory. Transfer-matrix (T-matrix) simulations are used to provide illustrations; the mechanics behind these techniques are not discussed here but are documented in the literature [11-13].

2 Comparing theoretical and real-world superlenses

In order to compare theoretical performance with what is practically obtainable a reference lens is defined: the one-dimensional lens consists of three planar layers with arbitrary thicknesses of 2.5 nm, 5 nm and 2.5 nm, giving a total thickness of 10 nm. The outer layers are made of RHM, with $\varepsilon_r = \mu_r = 1$. The thicker, central layer has $\varepsilon_r = -\mu_r = -1$ and is an electrically left-handed material (ELHM). The lens is exposed to TM polarised i-line radiation and has similar performance to an ideal (electromagnetic) Veselago lens as all material dimensions are much less than this wavelength. Transmission and phase characteristics for the

lens are shown in Fig. 3. These show that the reference design is capable of phenomenal resolution, with transmitted intensity close to 1 even for $k_x/2\pi > 200\ \mu m^{-1}$. (This corresponds to resolution of wavelengths smaller than 5 nm at the chosen wavelength of operation, $\lambda_0 = 365$ nm). There is a small glitch in transmitted intensity around $k_x/2\pi \approx 2.7\ \mu m^{-1}$ (corresponding to $\lambda = \lambda_0$) and a resonant peak forms at extremely high wave-numbers ($k_x/2\pi > 200\ \mu m^{-1}$). Both of these features are due to the electrostatic approximation ($\varepsilon_r = -1$, $\mu_r = 1$) and are not present in simulations where μ_r is equal to ε_r.

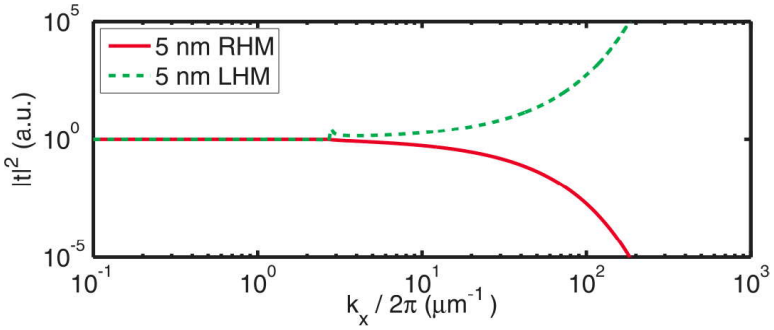

Fig. 2: Transmission characteristics for slabs of equal thickness with positive (RHM) and negative (LHM) ε_r.

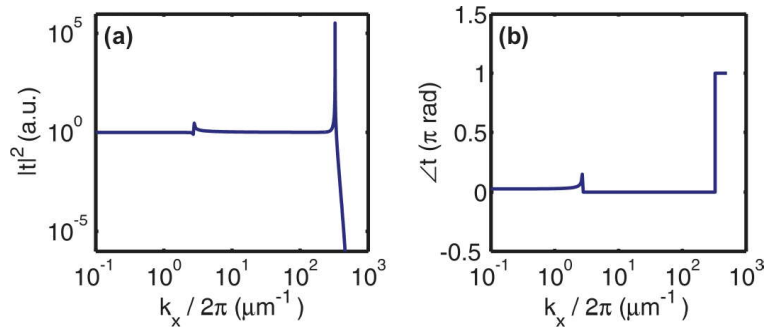

Fig 3: (a) Intensity and (b) phase characteristics of a 10 nm thick ideal electrostatic Veselago lens. Lens parameters are as shown in Fig. 1, however, $\varepsilon_r = 1$ for all media.

Several alterations to this reference design are now necessary to model lenses that can be fabricated with current technology. Firstly, the electrical and magnetic properties of the media are altered while their thicknesses are kept the same as those used in the reference design. Silver is chosen as an approximation to the ideal ELHM, as per Pendry's advice [2]. Poly(methyl methacrylate) (PMMA) is chosen as the RHM between the object and the ELHM, given that the magnitude of its permittivity ($\varepsilon_{r\ PMMA} = 2.3$) is close to that of silver ($\varepsilon_{r\ Ag} = -2.7 + 0.23i$) at λ_0 [14]. Furthermore, PMMA is desirable for its compatibility with the reactive ion etching (RIE) process required to generate mask patterns above the lens. Silicon dioxide (SiO_2), with $\varepsilon_{r\ SiO_2} = 2.368 + 0i$, is chosen instead of PMMA as the second RHM, due to better consistency during the fabrication process [9]. The effects of these real-world materials on the reference design are shown in Fig. 4a. The bandwidth of the lens is reduced to $k_x/2\pi \approx 100\ \mu m^{-1}$ (10 nm resolution), due to the loss represented by the complex part of $\varepsilon_{r\ Ag}$ [15]. The high-wave-number resonant peak is almost completely attenuated for the same reason and the λ_0-related glitch is shifted slightly towards higher wave numbers.

Despite these alterations, the transfer function is still reasonably flat in the pass band and would give much improved performance over a similarly dimensioned conventional lens.

A second approximation to our reference lens is now considered: the dimensions of the layers are stretched to mimic the experimental lenses described in the literature. To isolate the effects of these enlarged dimensions, the permittivities of the lens' constituent layers are left identical to those of the reference design. The thickness of the ELHM is set at 50 nm, or ten times the thickness in the reference design, as this is the minimum thickness at which silver was grown with appropriate roughness characteristics [9]. Accordingly, the thickness of the first RHM is set to 25 nm. The thickness of the final RHM is fixed at 10 nm, due to process constraints.

These changes have a much more dramatic effect on lens performance (Fig. 4b) than the changes to the material parameters in the previous example. Bandwidth is drastically reduced to $k_x/2\pi \approx 16\ \mu m^{-1}$ (62.5 nm resolution) and the glitch near λ_0 in the previous example is now a full-blown resonant peak. Critically, the transfer function in the region between this peak and the high wave number peak is no longer flat, reducing the likelihood of this lens faithfully reproducing sub-wavelength features. A cursory analysis suggests that these performance changes are due to the truncated final RHM layer; however, this only

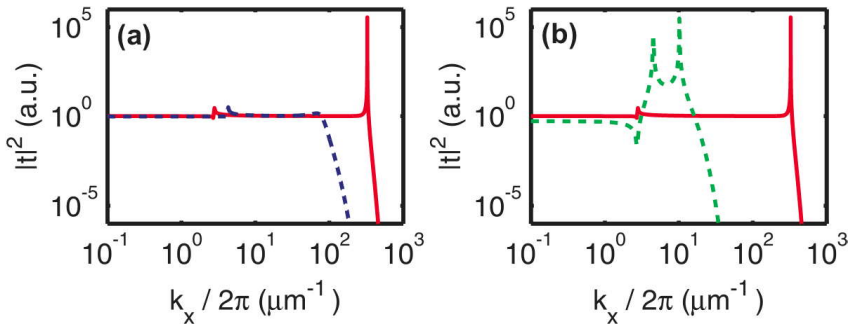

Fig 4: Transfer functions for the reference lens (solid) and (a) an actual material design (dashed). The behaviour of an actual thickness design (dashed) is shown in (b).

causes marginally higher transmission coefficients for extremely high wave numbers. This increase in transmission is too slight to be seen in Fig. 4b. Instead, the performance degradation is due mainly to the thick ELHM layer. At 50 nm, the thickness of the ELHM is more than 10% of λ_0, which falls outside the criteria for the electrostatic limit, which Pendry set as a prerequisite in his calculations [2].

Combining the electrical and physical alterations of the previous two simulations reveals an estimate of the likely performance available to a fabricated superlens: the transfer function for a 25/50/10 nm (PMMA/Ag/SiO_2 lens [9] is shown in Fig. 5. As before, the transfer function of the reference lens is shown for comparison. We can see that the dimensions of this lens dominate its bandwidth and the transfer function contains neither of the resonant peaks present in Fig 4b, thanks to the loss in the silver layer. Furthermore, the propagating part of the spectrum is uniformly attenuated, in a similar way and to a greater extent than in Fig 4b. We validate this estimate by comparing it to the actual performance observed in [9]. We see that the 145 nm periodic features that were resolved correspond to wave numbers around $k_x/2\pi \approx 6.7\ \mu m^{-1}$, which is close to the peak in transmission in our estimate.

These estimates not only explain the results achieved by experimental superlenses, but show why their performance is limited compared to the theoretical starting point that drives Pendry's research. We see that, of the approximations that Pendry makes, the electrostatic approximation is far stricter than the requirement for matching, lossless electrical characteristics. In terms of achieving a lens with a flat, broad transfer function it is much more important to reduce the limits on lens layer thickness than to find exactly matched permittivities in the layers that make up the lens. Furthermore, the loss in the silver layer is identified as a source of attenuation and smoothing of the resonant peaks in the transfer function. Attempts to manipulate these aspects to maximise resolution and fidelity are discussed in the next section.

3 Multilayer superlenses

We have shown that changing the dimensions and electrical properties of a superlens can alter the various features of its transfer function, namely bandwidth, resonant peaks, pass-band uniformity and low wave number attenuation. We see that performance degrades as we move away from the electrostatic limit, that is, as the dimensions of the component layers of our lens increase; and that loss is a convenient way of managing resonance. Ramakrishna *et al*. [15] came to similar conclusions via rigorous calculations in 2002; however, they explained deviation from the electrostatic limit in terms of the mismatch between $\varepsilon_{r\,Ag}$ and $\mu_{r\,Ag}$. They proposed a variation in $\varepsilon_{r\,Ag}$, rather than a variation in lens dimensions, as a solution to this problem. By carefully choosing $\varepsilon_{r\,RHM}$, they showed that the conditions for plasmon resonance could be met at different wavelengths. Increasing λ_0 would cause $\varepsilon_{r\,Ag}$ to be more negative, minimising the effects of the mismatch with $\mu_{r\,Ag}$.

Although feasible, this method did not catch on and is yet to be experimentally tested. Instead, considerable calculations [16,17] and simulations [18,19] have been used to study the effects of cascading individual superlenses into multilayer stacks. Instead of depositing all of the silver as one continuous layer in the superlens, several interleaved layers can be deposited, separated by similarly sized dielectric layers.

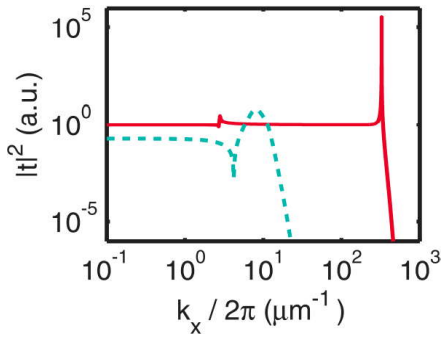

Fig. 5: Transfer functions for the reference lens (solid) and a practically achievable, 25/50/10 nm (PMMA/Ag/SiO_2 lens (dashed).

If the total silver thickness, Σt_{Ag}, is held constant as the number of metallo-dielectric layers increases, then the bandwidth will increase, too (Fig. 6). The benefit here comes not from the increasing number of metallo-dielectric layers, but from the shrinking layer dimensions that approach the electrostatic limit. Figure 7 shows what happens when the number of metallo-dielectric layers is increased without any decrease in

intra-layer dimensions: bandwidth, resonance and overall transmission all fall as the total lens thickness grows. This indicates a trade-off between bandwidth and resonance, and indicates that although repeated, thin lenses may give higher bandwidth than one thick lens, a single, thin lens will have the highest bandwidth of all. Finally, experimental work [20] has shown that most of the improvement in minimum resolution due to layer-halving (doubling the number of intra-lens silver layers while keeping Σt_{Ag} constant) is cancelled out by reduced pattern fidelity due to increased surface roughness on the constituent layers of the lens. Examples of line scans obtained at different object periods are shown in Fig. 8 [20]; these clearly show that increasing the number of silver layers in a lens is not a guaranteed way of increasing image fidelity.

4 Thick superlenses

These findings suggest that simply decreasing layer thickness or repeating layers within a stack are not enough to achieve a flat, non-resonant transfer function with large bandwidth. Furthermore, they do nothing to address the practical difficulties of growing very thin, smooth silver layers. Without thin layers we cannot begin to approach the electrostatic limit, and so we are prevented from achieving the diffraction-free imaging that Pendry describes. An alternative strategy is necessary: one where we abandon the pretense of operating near the electrostatic limit and enhancing the near field [21] in favour of engineering the surface plasmon resonance to achieve a better balance of transmission between the radiative and non-radiative parts of the spectrum.

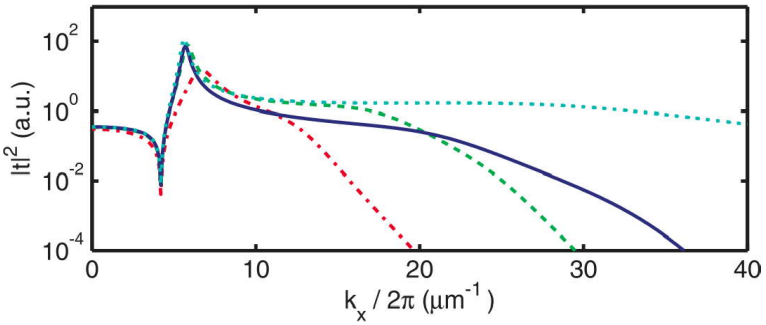

Fig. 6: Superlens designs with $\Sigma t_{Ag} = \Sigma t_{RHM} = 40$ nm. Designs consist of an initial dielectric layer (PMMA) followed by one (-·-), two (---), three (—) and eight (...) Ag-SiO_2 layer pairs. The initial and final layers are half as thick as all other layers in each case.

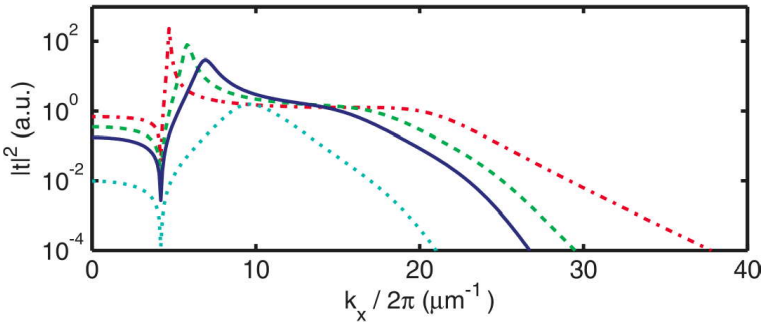

Fig 7: Superlens designs with $t_{Ag} = 20$ nm for each layer. The designs shown have one (-·-), two (---), three (—) and eight (...) silver layers, each separated by 20 nm of SiO_2. The initial layer is 10 nm thick PMMA, and the final layer is 10 nm thick SiO_2.

Instead of designing for thinner and thinner layers, we increase the thickness of the silver and dielectric layers to be such that the plasmon-mediated resonance, the loss in the silver and the evanescent decay in the dielectrics combine to give a flat, regular transfer function with reasonable bandwidth and limited resonant peaks. Furthermore, we aim to control the transmission ratio for propagating and evanescent terms, a parameter which has been identified as critical to lens fidelity in previous works [11, 22]. The price we pay for increasing lens thickness is broadband attenuation over a range of wave numbers; however, for lithography applications, this can be compensated by increasing the exposure time. The dimensions for such a spectrally balanced lens are shown in Fig. 9, with the corresponding transfer function shown in Fig. 10a.

The design process for this lens is as follows: firstly, an appropriate thickness for the silver layer is chosen. As silver initially beads during deposition due to surface tension [20] a film that is too thin will tend to have an inconsistent surface punctuated by holes or islands. On the other hand, a film that is too thick will have unsuitably high surface roughness [23] and strong DC attenuation. Hence, care is taken to grow a layer that is sufficiently uniform and smooth. Based on previous work [20], we choose the thickness of our silver layer to be 55 nm.

The next step involves setting the exposure time to achieve a fixed energy transfer, based on the DC transmission coefficient of the lens. As the loss in the dielectric layers is negligible, the DC transmission coefficient in our simulations is determined only by $\varepsilon_{r\,Ag}$ and t_{Ag}. (It is important to note that our simulations disregard the effects of reflection between the lens and any mask that is placed above it, these aspects will be addressed in a separate paper.) With $\varepsilon_{r\,Ag} = -2.7 + 0.23i$ and $t_{Ag} = 55$ nm, the DC transmission coefficient is calculated as 0.1447 (14%). In order to achieve the same energy transfer during the exposure step as we would when using an equivalent, lossless vacuum gap we increase the exposure time by a factor of $1 / 0.1447 \approx 6.9$.

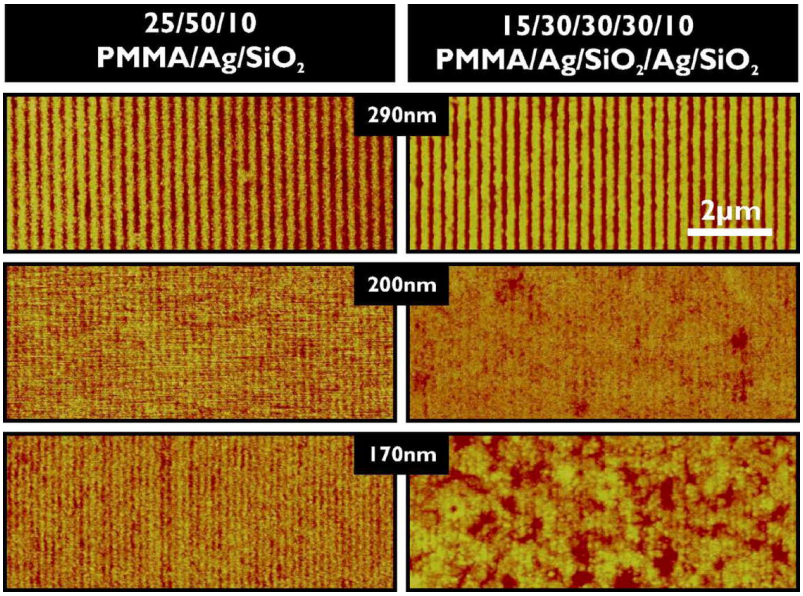

Fig 8: AFM line scans of periodic objects projected through single- (left) and double- (right) silver layer superlenses. Height scales for all images are 50 nm [20].

The third design step involves matching the peak evanescent transmission coefficient to the DC coefficient. As the silver thickness is now fixed, this parameter is controlled solely by the total thickness of dielectric surrounding the silver layer. The permittivities for the chosen dielectrics, $\varepsilon_{r\,PMMA} = 2.3013 + 0.0014i$ and $\varepsilon_{r\,SiO_2} = 2.368 + 0i$, are sufficiently close that altering the thickness of one is equivalent to altering the thickness of the other by the same amount. We fix the thickness of the SiO_2 layer, t_{SiO_2}, at 10 nm for compatibility with previous experiments [20] and thus choose the thickness of the PMMA layer, t_{PMMA}, to be 60 nm. This gives peak transmission of 0.1599 (16%) at $k_x/2\pi = 7.7$ ($\lambda \approx 130$ nm).

We measure the performance of this lens in terms of its bandwidth, which is defined as the range of wavelengths for which transmission is within 3 dB of the peak transmission coefficient (Fig. 10). Peak transmission in our case is 0.1599, corresponding to a cut-off transmission of 0.08. This gives a pass band from DC to $k_x/2\pi = 7.7$ and from $k_x/2\pi = 5.7$ to $k_x/2\pi = 9.2$ (corresponding to $\lambda_0\{\infty - 370, 175 - 109\}$ nm. Fig 10b depicts the transfer function for the fabricated lens shown in Fig. 5. Although the peak transmission is higher in this case (6.268 at $k_x/2\pi = 8.0$, or $\lambda \approx 125$ nm), the bandwidth is smaller, ranging only from $k_x/2\pi = 6.8$ to $k_x/2\pi = 9.7$ ($\lambda_0\{147 - 103\}$ nm). This increased bandwidth, which includes low wave numbers down to DC, shows that the DC-matched lens is an improvement over the previous state of the art. As an illustration, simulations of periodic patterns imaged through both lenses are shown in Fig. 11. The fabricated lens suffers from severe frequency doubling, which reduces the fidelity between the image and the object. The DC-matched lens is not affected to the same degree and clearly has better performance at this wavelength, despite the reduced intensity of its images.

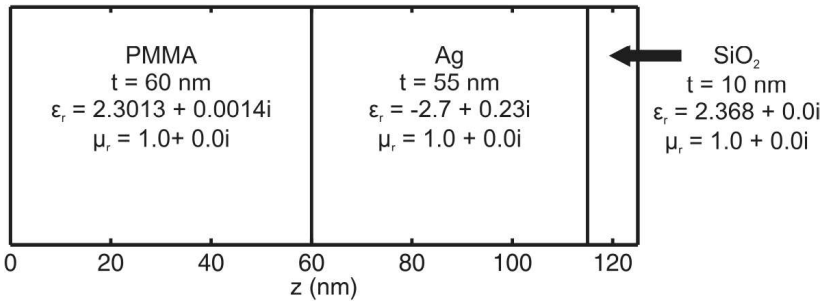

Fig 9: Dimensions and electromagnetic properties for a DC-matched superlens.

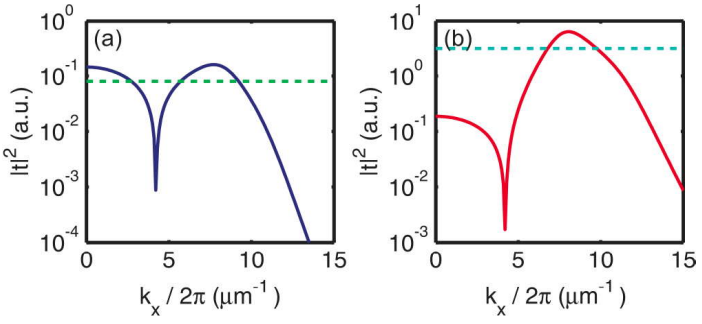

Fig 10: Lens transfer functions (solid) and –3 dB lines (dashed) for a DC-matched 60/55/10 nm PMMA/Ag/SiO_2 lens (a) and a practical 25/50/10 nm PMMA/Ag/SiO_2 lens (b).

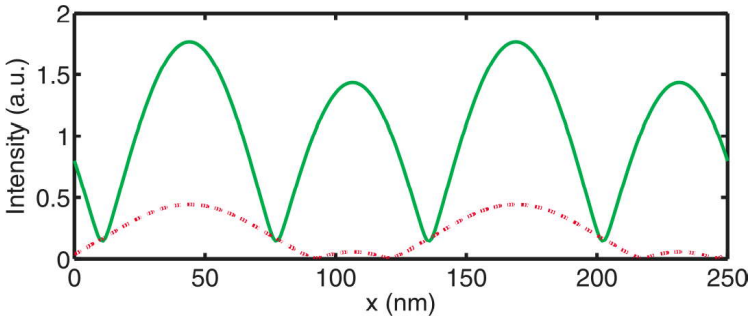

Fig 11: Image profiles for a DC-matched 60/55/10 nm PMMA/Ag/SiO_2 lens (---) and a practical 25/50/10 nm PMMA/Ag/SiO_2 lens (—). Input object is a 125 nm period square wave with amplitude = 1. λ_0 = 365 nm.

5 Conclusion

We have explored the development of superresolving silver lenses and have demonstrated the effects that physical dimensions and electromagnetic properties have on their transmission characteristics. We have shown that cascaded superlens layers do not result in intrinsically higher performance, as it is the thickness of individual layers, and not their number, that has the strongest effect on the evanescent waves of the near field. Lastly, we have shown that an appropriately engineered 'thick' superlens can achieve larger bandwidth and greater fidelity than superlenses that are currently realisable. Continued development of this work will see the techniques used for simulation refined to better account for mask-lens interactions, as well as surface roughness and layer thickness variations. Experimental verification of the thick superlens described here is also a priority.

Acknowledgement

CPM gratefully acknowledges financial support from the MacDiarmid Institute for Advanced Materials and Nanotechnology.

References

1. Veselago V G, *Sov Phys Usp*, 10 (1968) 759.
2. Pendry J B, *Phys Rev Lett*, 85 (2000) 3966.
3. Pendry J B, Holden A J, Stewart W J et al., *Phys Rev Lett*, 76 (1996) 4773.
4. Pendry J B, Holden A J, Robbins D J et al., *J Phys*, 10 (1998) 4785.
5. Pendry J B, Holden A J, Robbins D J et al., *IEEE Trans Microwave Theory Techniques*, 47 (1999) 2075.
6. Smith D R, Padilla W J, Vier D C et al., *Phys Rev Lett*, 84 (2000) 4184.
7. Shelby R A, Smith D R, Nemat-Nasser S C et al., *Appl Phys Lett*, 78 (2001) 489.
8. Shelby R A, Smith D R, Schultz S, *Science,* 292 (2001) 77.
9. Melville D O S, Blaikie R J, *Opt Express*, 13 (2005) 2127.
10. Fang N, Lee H, Sun C et al., *Science*, 308 (2005) 534.
11. Moore C P, Arnold M D, Bones P J et al., *J Opt Soc Am A*, 25 (2008) 911.
12. Melville D O S, PhD Thesis, University of Canterbury, New Zealand, (2006).
13. Moore C P, Arnold M D, Bones P J et al., *Proc 2008 Int Conf Nanosci Nanotechnol*, (2008) 210.
14. Johnson P B, Christy R W, *Phys Rev B*, 6 (1972) 4370.

15. Ramakrishna S A, Pendry J B, Schurig D et al., *J Mod Opt,* 49 (2002) 1747.
16. Ramakrishna S A, Pendry J B, Wiltshire M C K et al., *J Mod Opt*, 50 (2003) 1419.
17. Ramakrishna S A, Pendry J B, *Phys Rev B*, 67 (2003) 201101.
18. Shamonina E, Kalinin V A, Ringhofer K H et al., *Electron Lett*, 37 (2001) 1243.
19. Belov P A, Yang H, *Phys Rev B*, 73 (2006) 113110.
20. Melville D O S, Blaikie R J, *J Opt Soc Am B*, 23 (2006) 461.
21. Durant S, Fang N, Zhang X, *Appl Phys Lett*, 86 (2005) 126101.
22. Melville D O S, Blaikie R J, *Phys B*, 394 (2007) 197.
23. Kapaklis V, Poulopoulos P, Karoutsos V et al., *Thin Solid Films*, 510 (2006) 138.

[*Received:* 1.2.2009; *accepted* : 15.2.2009]